International Journal of Advances in Applied Sciences (IJAAS)
Vol. 15, No. 1, March 2026, pp. 313~321
ISSN: 2252-8814, DOI: 10.11591/ijaas.v15.i1.pp313-321

Hydrothermal synthesis of $ZnFe_2O_4$@g-C_3N_4 for enhanced adsorption-photocatalytic degradation of ciprofloxacin

Medya Ayunda Fitri[1], Muchammad Tamyiz[2], Eko Prasetyo Kuncoro[3], Mamlu'atul Nihaya[2], Muhammad Abdul Basith Thom Thom[2], Cindy Dwi Cahyani[1], Bahauddin Alqostolani[1]
[1]Department of Chemical Engineering, Faculty of Engineering, Universitas Nahdlatul Ulama Sidoarjo, Sidoarjo, Indonesia
[2]Department of Environmental Engineering, Faculty of Engineering, Universitas Nahdlatul Ulama Sidoarjo, Sidoarjo, Indonesia
[3]Environmental Engineering, Faculty of Sains and Technology, Universitas Airlangga, Surabaya, Indonesia

Article Info

Article history:

Received Sep 30, 2024
Revised Jan 25, 2026
Accepted Feb 17, 2026

Keywords:

Adsorption
Ciprofloxacin
Nanocomposite
Photocatalysis
ZF@2DCN

ABSTRACT

The persistence of antibiotic contaminants such as ciprofloxacin (CIP) in aquatic environments poses significant environmental and health risks, necessitating the development of efficient removal strategies. In this work, a zinc ferrite-anchored two-dimensional carbon nitride nanocomposite (ZF@2DCN) was synthesized via a simple calcination and hydrothermal approach to achieve synergistic adsorption–photocatalytic degradation of CIP under visible light. Structural and optical characterizations confirmed the successful formation of a ZF–2DCN heterojunction with high crystallinity, strong interfacial interactions, and enhanced visible-light absorption. The incorporation of ZF reduced the bandgap of 2DCN from 2.8 to 2.6 eV, promoting improved charge separation. Adsorption studies revealed rapid equilibrium within 30 min and multilayer adsorption on heterogeneous active sites, with a maximum adsorption capacity of 11.7 mg g^{-1}. Under visible-light irradiation, ZF@2DCN achieved up to 81% CIP degradation within 60 min, exhibiting an apparent reaction rate approximately 2.5 times higher than that of pristine 2DCN. The enhanced performance is attributed to the strong synergy between adsorption-driven pollutant enrichment and photocatalytic degradation. Overall, ZF@2DCN shows strong potential as an efficient material for antibiotic removal in wastewater treatment.

Corresponding Author:

Muchammad Tamyiz
Department of Environmental Engineering, Faculty of Engineering, Universitas Nahdlatul Ulama Sidoarjo
East Ring Road, KM 5.5 Rangkah Kidul, Sidoarjo District, Sidoarjo Regency, East Java 61234, Indonesia
Email: m_tamyiz@unusida.ac.id

1. INTRODUCTION

Pharmaceutical waste has led to growing concerns about water pollution, which is attracting more global focus. Ciprofloxacin (CIP), a commonly used antibiotic, is one of the primary contaminants. Its presence in wastewater contributes to antibiotic resistance and harms aquatic ecosystems. Conventional wastewater treatment techniques, including sedimentation, coagulation, and filtration, are largely ineffective in degrading antibiotics such as CIP [1], [2]. Therefore, developing more effective approaches for removing CIP from aqueous systems is critically important. Among the emerging approaches, photocatalysis has gained considerable attention as a viable treatment option. This technique offers several advantages for pollutant degradation, including low cost, high efficiency, environmental compatibility, and non-toxicity, while also minimizing the risk of secondary pollution [3]–[5]. This method has been successfully applied to the degradation of several antibiotics, such as sulfamethazine, enrofloxacin, and CIP [6]–[8]. In this context,

graphitic carbon nitride (g-C_3N_4 or CN) has attracted as a promising photocatalyst for applications including CO_2 reduction, water splitting, and pollutant degradation [9]. CN is especially appealing because of its appropriate bandgap of 2.7 eV, excellent stability, non-toxic nature, low cost, and suitability for large-scale production [10].

The conversion of bulk CN into ultrathin two-dimensional nanosheets (2DCN) results in a markedly increased surface area and reduced thickness relative to other CN architectures [11]. The enlarged surface area increases the availability of active sites and improves the separation efficiency of photogenerated electron–hole (e^-–h^+). Despite these advantages, 2DCN still exhibits intrinsic limitations, particularly weak visible-light absorption and inefficient charge-carrier separation, which restrict its overall photocatalytic performance [11]. One effective strategy to overcome these limitations is the construction of heterojunctions with complementary photocatalysts. Metal oxides, particularly bimetallic oxides, exhibit superior photocatalytic activity under visible light compared to single metal oxides [12]. Owing to their physicochemical stability and notable magnetic and optical properties, spinel ferrites, a class of bimetallic oxides, have gained increasing attention. In particular, zinc ferrite ($ZnFe_2O_4$ or ZF) has emerged as a promising material due to its sustainable synthesis, controllable stoichiometry, nanoscale dimensions, narrow bandgap (~1.9 eV), and scalability [13], [14].

Despite these merits, the photocatalytic efficiency of pristine ZF remains limited as a result of rapid recombination of photogenerated charge carriers [15]. This challenge can be effectively mitigated through heterojunction engineering. In the present work, a zinc ferrite-anchored two-dimensional carbon nitride nanocomposite (ZF@2DCN) nanocomposite was successfully fabricated via a hydrothermal approach, exhibiting a pronounced synergistic effect between adsorption and photocatalysis for CIP degradation. The incorporation of ZF narrowed the bandgap of 2DCN from 2.83 to 2.60 eV, thereby extending light absorption and enhancing CIP photodegradation. The ZF@2DCN nanocomposite exhibited are highly suitable for environmental applications and provides a new direction for the application of composite materials in environmental technology.

2. RESEARCH METHOD

2.1. Material

All reagents used in the fabrication of ZF@2DCN were of analytical grade and were utilized without any additional purification steps. The precursor materials included CH_4N_2O, $C_2H_4N_4$, $Zn(NO_3)_2{\cdot}6H_2O$, $C_5H_{12}O$, $C_{18}H_{34}O_2$, $C_{18}H_{37}N$, C_2H_5OH, C_6H_{14}, $Fe(NO_3)_3{\cdot}9H_2O$, and $C_{17}H_{18}FN_3O_3$. Ultrapure water (18.2 MΩ·cm) was used for the preparation of all aqueous solutions.

2.2. Synthesis of ZF@2DCN nanocomposite

The bulk graphitic CN was synthesized using a mixture of urea and dicyandiamide in a 2:1 weight ratio, and was calcined in ambient air at 550 °C for 4 h using a controlled heating rate of 2 °C min^{-1}. 2DCN were subsequently produced through thermal exfoliation by heating bulk CN to 520 °C at a rate of 5 °C min^{-1} for 2 h. In parallel, ZF was synthesized using a hydrothermal approach. Briefly, a 2:1 molar mixture of $Fe(NO_3)_3{\cdot}9H_2O$ and $Zn(NO_3)_2{\cdot}6H_2O$ was prepared by dissolving the salts in deionized (DI) water with continuous stirring. Subsequently, 60 mL of $C_5H_{12}O$ was introduced as the organic phase, followed by the addition of $C_{18}H_{34}O_2$ and $C_{18}H_{37}N$ in an equimolar ratio. After adjusting the pH to 11 with NaOH, the mixture was stirred for 1 h to ensure homogeneity, and the resulting suspension was sealed in a 50 mL Teflon-lined autoclave and hydrothermally treated at 180 °C for 16 h. After completion of the reaction, the obtained ZF nanoparticles were thoroughly washed with a mixture of C_2H_5OH and C_6H_{14} (1:3, v/v) to eliminate residual organic species and impurities.

The synthesis of the nanocomposite began by mixing 300 mg of 2DCN with varying amounts of ZF in 15 mL of DI water. The purpose of this mixing was to ensure proper interaction between 2DCN and ZF, resulting in a nanocomposite with the desired properties. The suspension was magnetically stirred for 6 h to achieve a uniform dispersion, a critical step for ensuring the homogeneous distribution of ZF on the 2DCN surface. Subsequently, the mixture was transferred into a Teflon-lined autoclave (50 mL capacity) and subjected to hydrothermal treatment at 160 °C for 16 h to enhance the structural integrity of the resulting nanocomposite. This heating stage is essential as it facilitates the formation of strong bonds between 2DCN and ZF, while also ensuring the stability and performance of the material for its intended applications.

2.3. Characterization of ZF@2DCN nanocomposite

X-ray diffraction (XRD) analysis was performed using a Bruker D8 Advance diffractometer, while the surface morphology of the samples was examined by scanning electron microscopy (SEM) with a JEOL JSM-6490LV, which was equipped with an energy-dispersive X-ray (EDX) spectrometer

(JEOL Centurio). Additionally, transmission electron microscopy (TEM) analysis was conducted with a Hitachi S-3000N. The optical absorption properties of the materials were performed using a Hitachi U-4100 spectrophotometer. Functional group identification was analyzed with a Nicolet 6700 spectrometer.

2.4. Photocatalytic degradation experiments

Adsorption tests were conducted in the dark using 10 mL of CIP solution (10 mg L^{-1}) at neutral pH and 25±2 °C. The materials 2DCN, ZF, and ZF@2DCN were added at a dosage of 0.5 g L^{-1} to evaluate their adsorption behavior. Subsequently, photocatalytic experiments were performed under visible-light irradiation using eight lamps (8 W each). Residual CIP concentrations and adsorption capacities were quantified via a liquid chromatography instrument (Agilent 1200).

2.5. Adsorption kinetics and isotherm models

Adsorption rate, adsorption capacity, and reaction order are key parameters controlling adsorption kinetics. To investigate the adsorption behavior of CIP on the ZF@2DCN surface, Lagergren kinetic models were employed. The adsorption process was analyzed using the linearized forms of the pseudo-first-order ((PFO), as in (1)) and pseudo-second-order ((PSO), as in (2)) models.

$$ln(q_e - q_t) = ln\, q_e - K_1 t \quad (1)$$

$$\frac{t}{q_t} = \frac{1}{K_2 + q_e^2} + \frac{1}{q_e} t \quad (2)$$

In the kinetic equations, q_t represents the amount of CIP adsorbed at a given time, whereas q_e denotes the equilibrium adsorption capacity (mg g^{-1}). The rate constants K_1 and K_2 correspond to the PFO, min^{-1} and PSO, mg g^{-1} min^{-1} models, respectively. Adsorption isotherm analysis offers insight into the distribution of CIP molecules at the solid–liquid interface under equilibrium conditions, indicating whether adsorption occurs on homogeneous or heterogeneous surfaces. It also provides information on the nature of the active sites and clarifies whether the process follows monolayer or multilayer adsorption. To further examine the adsorption mechanism of the photocatalytic adsorbent, the nonlinear Sips (3) and Temkin (4) isotherm models were performed.

$$q_e = \frac{K_a (C_e)^n}{1 + K_a (C_e)^n} q_m \quad (3)$$

$$q_e = \frac{RT}{B_T} ln K_T C_e \quad (4)$$

Collectively, these models provide insight into the interaction mechanisms between the nanocomposite adsorbents and CIP during the adsorption process. In these expressions, K_a and n represent the adsorption capacity and adsorption intensity (L mg^{-1}), respectively. R denotes the universal gas constant, B_T refers to the Temkin isotherm constant (J mol^{-1}), and K_T is the Temkin binding constant (L g^{-1}), and T is the absolute temperature (K).

3. RESULTS AND DISCUSSION

3.1. The ZF@2DCN structural and optical properties

Figure 1 illustrates the structural and optical characterization of the ZF@2DCN nanocomposite using XRD, Fourier transform infrared (FT-IR), and Kubelka–Munk analysis. The XRD patterns shown in Figure 1(a) reveal characteristic peaks of diffraction peaks attributed to pristine 2DCN and ZF appear at 2θ values of 27.6° and 35.4°, assigned to the (002) and (311) planes, respectively [16], [17]. These peaks match well with standard Joint Committee on Powder Diffraction Standards (JCPDS) cards (No. 87-1526 for 2DCN and No. 89-1010 for ZF), confirming high crystallinity and phase purity, with no detectable impurity peaks. Additional diffraction peaks observed for the ZF@2DCN nanocomposite at 12.6°, 27.5°, 29.8°, 35.5°, 42.5°, 53.2°, 56.6°, and 62.5° are indexed to the (100), (002), (220), (311), (400), (422), (511), and (440) planes, respectively [18]–[20]. The decreased intensity of the 2DCN (002) peak indicates the successful anchoring of ZF onto the surface of 2DCN.

Figure 1(b) displays FT-IR spectra of 2DCN, ZF, and ZF@2DCN nanocomposite. Characteristic C–N stretching vibrations of the heptazine framework appear in the 1,150–1,700 cm^{-1} region with a distinct band at 812 cm^{-1} corresponding to heptazine ring bending, while the broad band at 3,000–3,500 cm^{-1} is attributed to N–H stretching. ZF exhibits infrared-active bands at 563 and 432 cm^{-1} associated with Fe–O and Zn–O stretching vibrations [21], [22], along with a band at 1,635 cm^{-1} related to surface hydroxyl

groups [23]. Enhanced absorption peaks at 812, 1,246, 1,416, and 1,557 cm^{-1} in ZF@2DCN indicate strong interactions between ZF and 2DCN. Figures 1(c) and 1(d) show diffuse reflectance spectra (DRS) and Kubelka–Munk plots of 2DCN, ZF, and ZF@2DCN. The estimated bandgap energies are 2.8 eV for 2DCN, 1.9 eV for ZF, and 2.6 eV for the ZF@2DCN. Both 2DCN and ZF@2DCN exhibit indirect bandgap behavior, while ZF shows a direct bandgap nature [24], [25]. The ZF@2DCN nanocomposite demonstrates enhanced visible-light absorption compared to pristine 2DCN, favoring improved generation of photoinduced e^{-}–h^{+} pairs.

The SEM was employed to investigate the surface morphology of the samples, as presented in Figure 2. Pristine 2DCN (Figure 2(a)) displays a typical layered structure, whereas ZF nanoparticles (Figure 2(b)) show an almost spherical morphology with an average particle size of about 20 nm. As seen in Figure 2(c), the ZF nanoparticles are uniformly dispersed across the 2DCN surface, indicating the successful formation of the ZF@2DCN heterojunction.

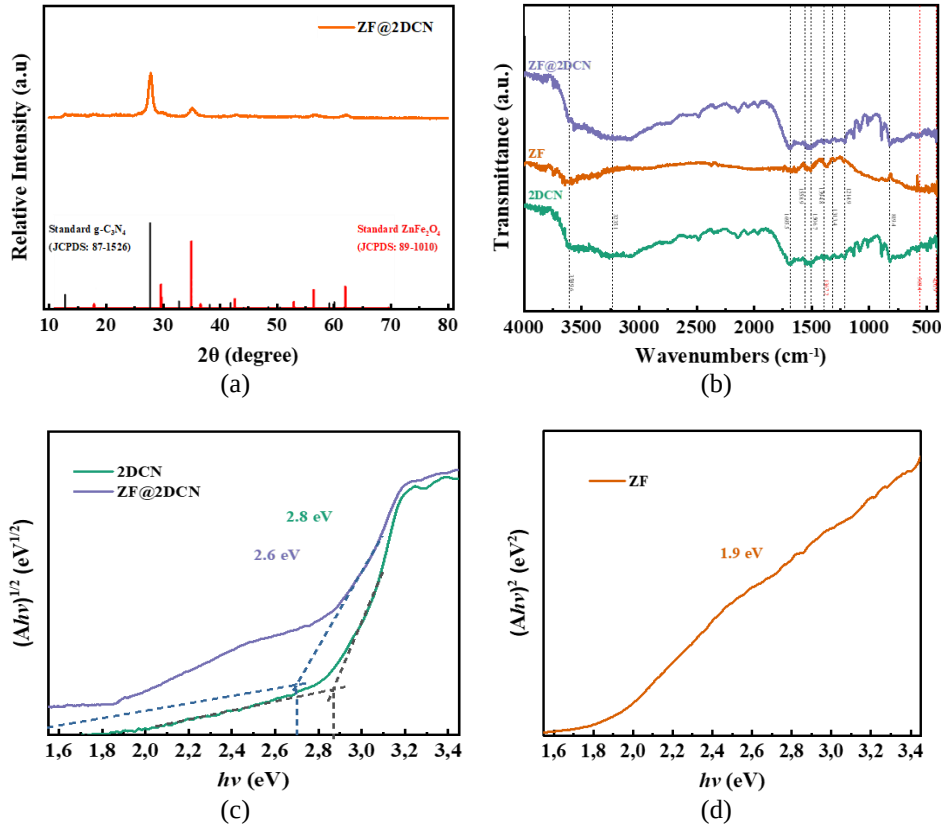

Figure 1. Structural and optical characterization of (a) XRD profile, (b) FT-IR spectroscopy spectra, (c) Kubelka–Munk plot of 2DCN and ZF, and (d) Kubelka–Munk plot of ZF@2DCN

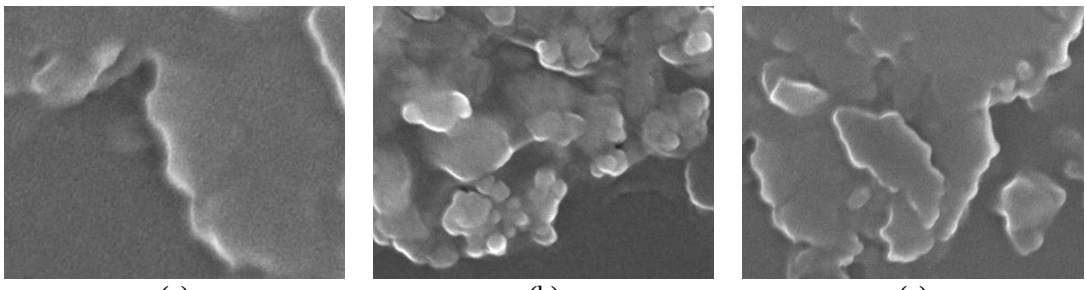

(a) (b) (c)

Figure 2. SEM images of (a) 2DCN, (b) ZF, and (c) ZF@2DCN nanocomposite

3.2. Synergistic adsorption–photocatalytic degradation of ciprofloxacin

The combined effect of adsorption-photodegradation of CIP over the ZF@2DCN was systematically evaluated with and without lamp exposure. Initial adsorption tests were carried out in the dark with a 10 mg L^{-1} CIP solution (10 mL, pH 7) to eliminate any photocatalytic contribution. Adsorption equilibrium was reached within 30 min. Figures 3-5 present the adsorption kinetics fitted using the PSO model, along with the photocatalytic degradation performance of 2DCN, ZF, and ZF@2DCN, as well as the Sips isotherm fitting results. As shown in Figure 3, CIP adsorption occurs rapidly within the first 10 min, followed by a slower progression toward equilibrium. Among the tested materials, ZF@2DCN exhibits the highest adsorption capacity (6.8 mg g^{-1}), corresponding to CIP removal efficiencies of 31% and 21%, whereas pristine 2DCN shows a lower adsorption capacity of 4.6 mg g^{-1} with 21% removal. In contrast, ZF demonstrates a significantly lower adsorption capacity of 2.7 mg g^{-1}, achieving only 12% CIP removal.

Owing to its narrow bandgap (1.9 eV), ZF experiences pronounced recombination of photogenerated (e^-–h^+) pairs, leading to the weakest photocatalytic performance, with only 16% CIP degradation achieved within 30 min (Figure 4). In contrast, 2DCN and ZF@2DCN display substantially enhanced photocatalytic activities, attaining CIP removal efficiencies of 32% and 53%, respectively. The superior performance of the ZF@2DCN nanocomposite is primarily attributed to its reduced bandgap energy (2.6 eV) compared with pristine 2DCN (2.8 eV), which improves visible-light absorption and effectively suppresses charge-carrier recombination. Notably, ZF@2DCN achieves up to 81% CIP degradation within 60 min, underscoring its excellent photocatalytic efficiency. The photocatalytic degradation of CIP follows PSO kinetics, and the superior reaction rate of ZF@2DCN arises from the synergistic coupling of adsorption and photocatalysis. In this system, CIP molecules are preferentially adsorbed and concentrated on the lamellar 2DCN matrix, which provides a large surface area and abundant mesoporous sites. This adsorption-driven enrichment facilitates rapid CIP depletion in solution and enhances the probability of interaction with photo-generated reactive oxygen species, thereby accelerating photodegradation. These findings demonstrate that the formation of a ZF-2DCN heterojunction plays a critical role in enhancing photocatalytic performance, rendering ZF@2DCN highly effective for CIP removal.

Based on the calculated apparent rate constants (0.0127, 0.0014, and 0.0053 min^{-1} for ZF@2DCN, ZF, and 2DCN, respectively), the ZF@2DCN nanocomposite demonstrates a degradation rate nearly 2.5 times higher than that of pristine 2DCN. Moreover, the higher distribution coefficient (K_d) and rate constant values further highlight the strong synergistic interaction between adsorption and photocatalysis. The adsorption behavior of CIP was further investigated over an initial concentration range of 5–50 mg L^{-1}. Equilibrium was attained within 30 min, during which the adsorption capacity increased with rising CIP concentration until saturation occurred. Corresponding equilibrium capacities were 4.7–10.8 mg g^{-1} for Initial CIP concentrations between 5 and 50 mg L^{-1}. Both experimental results and kinetic modeling indicate that the concentration-dependent adsorption behavior follows the PSO model, suggesting a process of multilayer adsorption. According to the classification of Giles and Smith, the resulting adsorption isotherm of CIP on ZF@2DCN is identified as an L_2-type, indicating a strong affinity between the adsorbent and adsorbate through chemical bonding or electrostatic interactions in a multilayer adsorption system. These results confirm that CIP adsorption on the ZF@2DCN nanocomposite occurs on heterogeneous active sites via a multilayer mechanism [26]–[28]. To further elucidate the adsorption behavior, the Sips isotherm model was applied (Figure 5). This hybrid model, which integrates the Langmuir and Freundlich theories for heterogeneous surfaces, shows an excellent fit with an R^2 value of 0.975 and yields a maximum adsorption capacity of 11.7 mg g^{-1} [29], [30]. These findings confirm that CIP adsorption on the ZF@2DCN nanocomposite occurs on heterogeneous active sites via a multilayer adsorption mechanism.

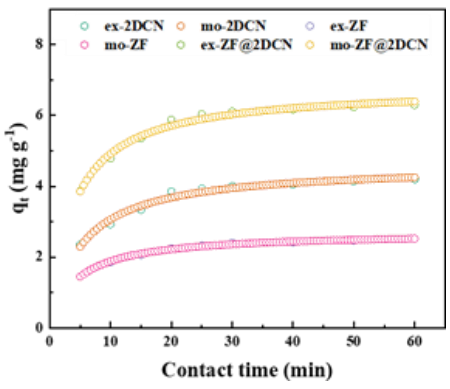

Figure 3. Adsorption and photocatalytic analysis of adsorption kinetics and PSO exponential fitting

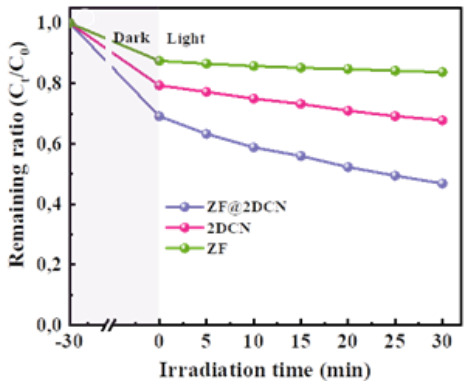

Figure 4. Adsorption and photocatalytic analysis of photocatalytic performance of 2DCN, ZF, and the ZF@2DCN nanocomposite

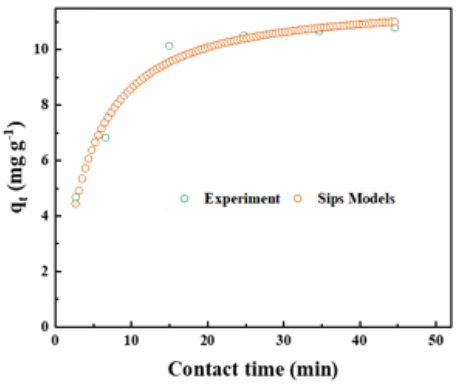

Figure 5. Adsorption and photocatalytic analysis of Sips isotherm exponential fitting

4. CONCLUSION

A ZF@2DCN nanocomposite was successfully developed and demonstrated outstanding performance for the synergistic adsorption–photocatalytic degradation of CIP under visible light. Structural and optical analyses confirmed effective ZF anchoring on 2DCN, leading to enhanced visible-light absorption and reduced bandgap energy (2.6 eV), which promoted efficient charge separation. The ZF@2DCN nanocomposite exhibited rapid adsorption equilibrium, multilayer adsorption on heterogeneous active sites, and a maximum adsorption capacity of 11.7 mg g^{-1}. Notably, it achieved up to 81% CIP degradation within 60 min, with an apparent reaction rate approximately 2.5 times higher than that of pristine 2DCN. The enhanced performance arises from the strong synergy between adsorption-driven pollutant enrichment and photocatalytic degradation at the ZF–2DCN heterojunction. These findings highlight ZF@2DCN as a promising photocatalyst for the efficient removal of antibiotic contaminants from wastewater.

FUNDING INFORMATION

The author would like to express gratitude to the Directorate of Research and Community Service, Deputy for Research and Development Strengthening, Ministry of Education, Culture, Research, and Technology, for their financial support in accordance with the 2024 Fiscal Year Research Contract Number: 109/E5/PG.02.00.PL/2024.

AUTHOR CONTRIBUTIONS STATEMENT

This journal uses the Contributor Roles Taxonomy (CRediT) to recognize individual author contributions, reduce authorship disputes, and facilitate collaboration.

Name of Author	C	M	So	Va	Fo	I	R	D	O	E	Vi	Su	P	Fu
Medya Ayunda Fitri	✓	✓	✓		✓			✓	✓		✓			
Muchammad Tamyiz	✓			✓	✓		✓	✓	✓	✓				✓
Eko Prasetyo Kuncoro		✓	✓		✓	✓		✓	✓					
Mamlu'atul Nihaya		✓	✓					✓	✓					
Muhammad Abdul Basith Thom Thom		✓	✓		✓				✓					
Cindy Dwi Cahyani			✓		✓			✓	✓		✓			
Bahauddin Alqostolani			✓		✓			✓	✓		✓			

C : **C**onceptualization
M : **M**ethodology
So : **So**ftware
Va : **Va**lidation
Fo : **Fo**rmal analysis
I : **I**nvestigation
R : **R**esources
D : **D**ata Curation
O : Writing - **O**riginal Draft
E : Writing - Review & **E**diting
Vi : **Vi**sualization
Su : **Su**pervision
P : **P**roject administration
Fu : **Fu**nding acquisition

CONFLICT OF INTEREST STATEMENT

The authors declare that they have no known competing financial interests or personal relationships that could have appeared to influence the work reported in this paper.

INFORMED CONSENT

We have obtained informed consent from all individuals included in this study.

ETHICAL APPROVAL

The research related to human use has been complied with all the relevant national regulations and institutional policies in accordance with the tenets of the Helsinki Declaration and has been approved by the authors' institutional review board or equivalent committee.

DATA AVAILABILITY

The data that support the findings of this study are available from the corresponding author, [MT], upon reasonable request.

REFERENCES

[1] J. Sha *et al.*, "Diametrically opposite effect of Cu^{2+} on sulfamerazine and ciprofloxacin adsorption-photodegradation in g-C_3N_4/visible light system: behavior and mechanism study," *Chemical Engineering Journal*, vol. 428, Jan. 2022, doi: 10.1016/j.cej.2021.131065.

[2] R. Rafieenia, M. Sulonen, M. Mahmoud, F. El-Gohary, and C. A. Rossa, "Integration of microbial electrochemical systems and photocatalysis for sustainable treatment of organic recalcitrant wastewaters: main mechanisms, recent advances, and present prospects," *Science of The Total Environment*, vol. 824, Jun. 2022, doi: 10.1016/j.scitotenv.2022.153923.

[3] P. Wang, Y. Tang, Z. Dong, Z. Chen, and T.-T. Lim, "Ag–AgBr/TiO_2/RGO nanocomposite for visible-light photocatalytic degradation of penicillin G," *Journal of Materials Chemistry A*, vol. 1, no. 15, pp. 4718–4727, 2013, doi: 10.1039/c3ta01042b.

[4] R. Zhang, J. Jiang, and K. Zeng, "Synthesis of Bi_2WO_6/g-C_3N_4 heterojunction on activated carbon fiber membrane as a thin-film photocatalyst for treating antibiotic wastewater," *Inorganic Chemistry Communications*, vol. 140, Jun. 2022, doi: 10.1016/j.inoche.2022.109418.

[5] J. Zhang, Y. Zheng, H. Zheng, T. Jing, Y. Zhao, and J. Tian, "Porous oxygen-doped g-C_3N_4 with the different precursors for excellent photocatalytic activities under visible light," *Materials*, vol. 15, no. 4, Feb. 2022, doi: 10.3390/ma15041391.

[6] V. D. Dang *et al.*, "Indirect Z-scheme nitrogen-doped carbon dot decorated Bi_2MoO_6/g-C_3N_4 photocatalyst for enhanced visible-light-driven degradation of ciprofloxacin," *Chemical Engineering Journal*, vol. 422, Oct. 2021, doi: 10.1016/j.cej.2021.130103.

[7] P. Zhou *et al.*, "Nitrogen-defect-modified g-C_3N_4/$BaFe_{12}O_{19}$ S-scheme heterojunction photocatalyst with enhanced advanced oxidation technology synergistic photothermal degradation ability of antibiotic: insights into performance, electron transfer pathways and toxicity," *Applied Catalysis B: Environmental*, vol. 343, Apr. 2024, doi: 10.1016/j.apcatb.2023.123485.

[8] P. Chen, S. Di, X. Qiu, and S. Zhu, "One-step synthesis of F-TiO_2/g-C_3N_4 heterojunction as highly efficient visible-light-active catalysts for tetrabromobisphenol A and sulfamethazine degradation," *Applied Surface Science*, vol. 587, Jun. 2022, doi: 10.1016/j.apsusc.2022.152889.

[9] H. D. A. Kader, S. H. Ammar, W. A. Abdulnabi, Z. H. Jabbar, H. Taofeeq, and A. Al-Farraji, "Enhancing visible-light-based photodegradation of antibiotics over facile constructed $BiVO_4$/S-doped g-C_3N_4 heterojunctions in an airlift photocatalytic reactor," *Journal of Water Process Engineering*, vol. 65, Aug. 2024, doi: 10.1016/j.jwpe.2024.105900.

[10] P. J. Mafa *et al.*, "Multi-elemental doped g-C_3N_4 with enhanced visible light photocatalytic activity: insight into naproxen degradation, kinetics, effect of electrolytes, and mechanism," *Separation and Purification Technology*, vol. 282, Feb. 2022, doi: 10.1016/j.seppur.2021.120089.

[11] X. Deng *et al.*, "Boosting interfacial charge separation and photocatalytic activity of 2D/2D g-C_3N_4/$ZnIn_2S_4$ S-scheme heterojunction under visible light irradiation," *Journal of Alloys and Compounds*, vol. 894, Feb. 2022, doi: 10.1016/j.jallcom.2021.162209.

[12] Y. Zhang *et al.*, "CNTs boosting superior cycling stability of $ZnFe_2O_4$/C nanoparticles as high-capacity anode materials of Li-ion batteries," *Journal of Alloys and Compounds*, vol. 912, Aug. 2022, doi: 10.1016/j.jallcom.2022.165135.

[13] H. Yang *et al.*, "An efficient construction method of S-scheme Ag_2CrO_4/$ZnFe_2O_4$ nanofibers heterojunction toward enhanced photocatalytic and antibacterial activity," *Colloids and Surfaces A: Physicochemical and Engineering Aspects*, vol. 641, May 2022, doi: 10.1016/j.colsurfa.2022.128603.

[14] X. Wu, J. Lu, S. Huang, X. Shen, S. Cui, and X. Chen, "Facile fabrication of novel magnetic 3-D $ZnFe_2O_4$/ZnO aerogel based heterojunction for photoreduction of Cr(VI) under visible light: controlled synthesis, facial change distribution, and DFT study," *Applied Surface Science*, vol. 594, Aug. 2022, doi: 10.1016/j.apsusc.2022.153486.

[15] J. Luo *et al.*, "Synergistic adsorption-photocatalytic activity using Z-scheme based magnetic $ZnFe_2O_4$/$CuWO_4$ heterojunction for tetracycline removal," *Journal of Alloys and Compounds*, vol. 910, Jul. 2022, doi: 10.1016/j.jallcom.2022.164954.

[16] S. Wang and J. Wang, "Magnetic 2D/2D oxygen doped g-C_3N_4/biochar composite to activate peroxymonosulfate for degradation of emerging organic pollutants," *Journal of Hazardous Materials*, vol. 423, Feb. 2022, doi: 10.1016/j.jhazmat.2021.127207.

[17] Y. Wu, J. Chen, H. Che, X. Gao, Y. Ao, and P. Wang, "Boosting 2e−oxygen reduction reaction in garland carbon nitride with carbon defects for high-efficient photocatalysis-self-Fenton degradation of 2,4-dichlorophenol," *Applied Catalysis B: Environment and Energy*, vol. 307, Jun. 2022, doi: 10.1016/j.apcatb.2022.121185.

[18] T. B. Nguyen, C. P. Huang, and R. Doong, "Photocatalytic degradation of bisphenol A over a $ZnFe_2O_4$/TiO_2 nanocomposite under visible light," *Science of The Total Environment*, vol. 646, pp. 745–756, Jan. 2019, doi: 10.1016/j.scitotenv.2018.07.352.

[19] A. I. Al-Sulami, M. H. Alsuwat, F. M. H. AlSulami, A. M. Ibrahim, and A. A. Elhenawy, "$ZnFe_2O_4$/bentonite/polyacrylamide: exploring structural properties for removal of Alizarin yellow dye and antibacterial activities," *Colloids and Surfaces A: Physicochemical and Engineering Aspects*, vol. 687, Apr. 2024, doi: 10.1016/j.colsurfa.2024.133408.
[20] H. A. Al-Shwaiman *et al.*, "Fabrication of intimately coupled CeO_2/$ZnFe_2O_4$ nano-heterojunction for visible-light photocatalysis and bactericidal application," *Materials Chemistry and Physics*, vol. 279, Mar. 2022, doi: 10.1016/j.matchemphys.2022.125759.
[21] P. R. Matli, X. Zhou, D. Shiyu, and Q. Huang, "Fabrication, characterization, and magnetic behavior of porous $ZnFe_2O_4$ hollow microspheres," *International Nano Letters*, vol. 5, no. 1, pp. 53–59, Mar. 2015, doi: 10.1007/s40089-014-0135-2.
[22] T. B. Nguyen and R. Doong, "Heterostructured $ZnFe_2O_4$/TiO_2 nanocomposites with a highly recyclable visible-light-response for bisphenol A degradation," *RSC Advances*, vol. 7, no. 79, pp. 50006–50016, 2017, doi: 10.1039/C7RA08271A.
[23] E. Sarala, M. M. Naik, M. Vinuth, Y. V. R. Reddy, and H. R. Sujatha, "Green synthesis of Lawsonia inermis-mediated zinc ferrite nanoparticles for magnetic studies and anticancer activity against breast cancer (MCF-7) cell lines," *Journal of Materials Science: Materials in Electronics*, vol. 31, no. 11, pp. 8589–8596, Jun. 2020, doi: 10.1007/s10854-020-03394-8.
[24] P. Sarkar, S. De, and S. Neogi, "Microwave assisted facile fabrication of dual Z-scheme g-C_3N_4/$ZnFe_2O_4$/Bi_2S_3 photocatalyst for peroxymonosulphate mediated degradation of 2,4,6-Trichlorophenol: the mechanistic insights," *Applied Catalysis B: Environment and Energy*, vol. 307, Jun. 2022, doi: 10.1016/j.apcatb.2022.121165.
[25] Y. Shi *et al.*, "Engineering of 2D/3D architectures type II heterojunction with high-crystalline g-C_3N_4 nanosheets on yolk-shell $ZnFe_2O_4$ for enhanced photocatalytic tetracycline degradation," *Materials Research Bulletin*, vol. 150, Jun. 2022, doi: 10.1016/j.materresbull.2022.111789.
[26] M. A. Abbasi *et al.*, "Synergetic effect of adsorption-photocatalysis by GO-C_eO_2 nanocomposites for photodegradation of doxorubicin" *Journal of Environmental Chemical Engineering*, vol. 10, no. 1, Feb. 2022, doi: 10.1016/j.jece.2021.107078.
[27] P. Wang *et al.*, "Silica coated Fe_3O_4 magnetic nanospheres for high removal of organic pollutants from wastewater," *Chemical Engineering Journal*, vol. 306, pp. 280–288, Dec. 2016, doi: 10.1016/j.cej.2016.07.068.
[28] J. Li, B. Li, H. Huang, N. Zhao, M. Zhang, and L. Cao, "Investigation into lanthanum-coated biochar obtained from urban dewatered sewage sludge for enhanced phosphate adsorption," *Science of The Total Environment*, vol. 714, Apr. 2020, doi: 10.1016/j.scitotenv.2020.136839.
[29] J. Wang and X. Guo, "Adsorption isotherm models: classification, physical meaning, application and solving method," *Chemosphere*, vol. 258, Nov. 2020, doi: 10.1016/j.chemosphere.2020.127279.
[30] Q. Zhou, W. Chen, X. Jiang, H. Liu, S. Ma, and B. Wang, "Preparation of a novel nitrogen-containing graphitic mesoporous carbon for the removal of acid red 88," *Scientific Reports*, vol. 10, no. 1, Jan. 2020, doi: 10.1038/s41598-020-57823-z.

BIOGRAPHIES OF AUTHORS

Medya Ayunda Fitri is a lecturer in the Chemical Engineering Study Program at Nahdlatul Ulama University, Sidoarjo. Her field of expertise is the process of mass and heat transfer. Her research interest includes mass and heat transfer, bioenergy, waste treatment, and materials. She is a Master's graduate from the Chemical Engineering Department of the Sepuluh Nopember Institute of Technology, Surabaya. She can be contacted at email: medyafitri.tkm@unusida.ac.id.

Muchammad Tamyiz is a Ph.D. in International Ph.D. Program in Environmental Science and Technology from National Tsing Hua University (NTHU), Taiwan in 2023, Magister Sains (M.Si) (Chemistry) (Institut Teknologi Sepuluh Nopember (ITS), Indonesia, Sarjana Sains (Chemistry) (Universitas Negeri Surabaya, Indonesia). His research interest includes advanced oxidation processes, environmental chemistry, environmental nanotechnology, wastewater treatment, and water technology. He can be contacted at email: m_tamyiz.tkl@unusida.ac.id.

Eko Prasetyo Kuncoro is a lecturer in Environmental Engineering, Faculty of Science and Technology at Universitas Airlangga, Surabaya, Indonesia. He received doctor degree in Environmental Science and Engineering from Ecole Nationale Superieure des Mines de Saint-Etienne-Universite Jean Monnet de Saint-Etienne, France in 2005. His research interest includes sustainable transformation materials and energy, pollution prevention and control, waste, and hazardous waste management. He can be contacted at email: eko-p-k@fst.unair.ac.id.

Mamlu'atul Nihaya is a student in the Department of Environmental Engineering at Nahdlatul Ulama University, Sidoarjo. Her academic interests focus on the study of environmental systems and engineering-based solutions. She can be contacted at email: mamlu.yaya001@gmail.com.

Muhammad Abdul Basith Thom Thom is a student in the Department of Environmental Engineering at Nahdlatul Ulama University, Sidoarjo. His academic interest is in environmental management and sustainable solutions for environmental problems. He can be contacted at email: abeelike01@gmail.com.

Cindy Dwi Cahyani is a student in the Department of Chemical Engineering at Nahdlatul Ulama University, Sidoarjo. Her academic interest includes chemical process analysis and the application of chemical engineering principles. She can be contacted at email: cindydwicahyani17@gmail.com.

Bahauddin Alqostolani is a student in the Department of Chemical Engineering at Nahdlatul Ulama University, Sidoarjo. His interest focuses on chemical engineering fundamentals and their implementation in academic and applied studies. He can be contacted at email: bahauddin.alqostolani29@gmail.com.